Spatial Separation of β-Sheet Domains of β-Amyloid: Disruption of Each β-Sheet by *N*-Methyl Amino Acids†

Kimberly L. Sciarretta,‡ Adrienne Boire,§ David J. Gordon,§ and Stephen C. Meredith*,§,||

Departments of Molecular Genetics and Cell Biology, Biochemistry and Molecular Biology, and Pathology, The University of Chicago, Chicago, Illinois 60637

Received March 21, 2006; Revised Manuscript Received May 10, 2006

ABSTRACT: In a recent model of β-amyloid (Aβ) fibrils, based mainly on solid-state NMR data, a molecular layer consists of two β-sheets (residues 12−23 and 31−40 of Aβ1−40), folded onto one another by a connecting "bend" structure (residues 25−29) in the side-chain dimension. In this paper, we use two *N*-methyl amino acids to disrupt each of the two β-sheets individually (2NMe(NTerm), residues 17 and 19; and 2NMe(CTerm), residues 37 and 39), or both of them at the same time (4NMe, with the above four N-methylated residues). Our data indicate that incorporation of two *N*-methyl amino acids into one β-sheet is sufficient to disrupt that sheet while leaving the other, unmodified β-sheet intact and able to form fibrils. We show, however, that disruption of each of the two β-sheets has strikingly different effects on fibrillogenesis kinetics and fibril morphology. Both 2NMe(NTerm) and 2NMe(CTerm) form fibrils at similar rates, but more slowly than that of unmodified Aβ1−40. Electron microscopy shows that 2NMe-(NTerm) forms straight fibrils with fuzzy amorphous material coating the edges, while 2NMe(CTerm) forms very regular, highly twisted fibrils—in both cases, distinct from the morphology of Aβ1−40 fibrils. Both 2NMe peptides show a "CMC" approximately four times greater than that of Aβ1−40. CD spectra of these peptides also evolve differently in time: whereas the CD spectra of 2NMe(NTerm) evolve little over 10 days, those of 2NMe(CTerm) show a transition to high β-sheet content at about day 4−5. We also show that disruption of both β-sheet domains, as in 4NMe, prevents fibril formation altogether, and renders Aβ1−40 highly water soluble and monomeric, and with solvent-exposed side chains. In summary, our data show (1) that the two β-sheet domains fold in a semiautonomous manner, since disrupting each one still allows the other to fold; (2) that disruption of the N-terminal β-sheet has a more profound effect on fibrillogenesis than disruption of the C-terminal β-sheet, suggesting that the former is the more critical for the overall structure of the fibril; and (3) that disruption of both β-sheet domains renders the peptide monomeric and unable to form fibrils.

Aβ[1] peptides, the major protein components of the amyloid core of neuritic plaques in Alzheimer's disease, spontaneously assemble into β-sheet rich amyloid fibrils in vitro. Solid-state NMR and other data (*1*−*4*) indicate that Aβ10−35 and Aβ1−40 form parallel β-sheets with all residues in register. Aβ10−35, Aβ1−40, and Aβ1−42 can be conceived as having four domains. An inspection of the amino acid sequence of Aβ1−42 shows two hydrophobic domains: residues 17−21, the hydrophobic "core" domain, and residues 31−42, the C-terminal hydrophobic domain. Solid-state NMR data indicate that both of these hydrophobic domains, and some of the amino acids directly adjacent to them, constitute the β-sheets of Aβ10−35 and Aβ1−40 amyloid fibrils, while the N-terminal nine amino acids remain unstructured in the fibril. Additional solid-state NMR data indicate that the β-sheets are interrupted by a highly structured but non-β-sheet region at amino acids 25−29 (*5*). A recent model (*5*−*7*) of the Aβ1−40 fibril based on solid-state NMR (*1*−*4*, *8*), electron microscopy (*9*), and X-ray diffraction (*10*) data proposed that the fibril consists of units of two spatially separated β-strands folded over one another to form a molecular double layer of β-sheets. The region connecting these β-sheets, $G_{25}SNKG_{29}$, allows the peptide chain to reverse direction, and for this reason it is sometimes referred to as the "bend region" (*5*, *11*). This is not a canonical β-turn, however, since, unlike typical turns, interactions between residues in the region are mainly between side chains, and not between backbone atoms (e.g., the hydrogen bonds typical of some β-turns). The bend brings the two β-sheets into close apposition, thereby creating a

† Funding was provided by American Federation of Aging Research (Glenn/AFAR, K.L.S.), NIH MCB Training Grant (NIH/NIGMS T32 GM07183, K.L.S.), NIH Medical Scientist Training Grant (5 T32 GM07281, D.J.G.), and NIH (RO1 NS042852, S.C.M.).

* Corresponding author. Mailing address: Department of Pathology, The University of Chicago, 5841 S. Maryland Ave., Chicago, IL 60637. Tel: 773-702-1267. Fax: 773-834-5251. E-mail: scmeredi@uchicago.edu.

‡ Department of Molecular Genetics and Cell Biology.

§ Department of Biochemistry and Molecular Biology.

|| Department of Pathology.

[1] Abbreviations: Aβ, β-amyloid; CD, circular dichroism; CMC, critical micelle concentration; DMSO, dimethyl sulfoxide; DPH, 1,6-diphenyl-1,3,5-hexatriene; ESI, electrospray ionization; λ_{EM}, emission wavelength; λ_{EX}, excitation wavelength; FMOC, 9-fluorenylmethoxycarbonyl; HPLC, high performance liquid chromatography; MALDI-TOF, matrix assisted laser desorption time-of-flight; NMe, *N*-methyl; NMR, nuclear magnetic resonance; THF, tetrahydrofuran; TFA, trifluoroacetic acid.

10.1021/bi0605585 CCC: $33.50
Published on Web 07/18/2006

hydrophobic pocket between the two β-sheets formed by their side chains.

This emerging model of Aβ1−40 fibrils—of a double layer of N- and C-terminal β-sheets interacting with one another in a hydrophobic pocket—raises the question of whether these two β-sheet regions can assemble into fibrils independently of one another. Short peptides with the sequence of the isolated hydrophobic domains of Aβ form fibrils (*12*, *13*), but in the case of Aβ16−22, encompassing the hydrophobic core domain of Aβ, the fibrils differ drastically from those of the full length peptide, i.e., antiparallel and in-register parallel β-sheets for Aβ16−22 and Aβ1−40, respectively. In this paper, we ask whether each of the future β-sheets of Aβ1−40 can form in the context of a full length Aβ peptide when the other is focally disrupted. Our strategy was to disrupt each of the two individual β-sheets of Aβ1−40 by incorporating site-specific *N*-methyl amino acids. We (*14*−*16*) and others (*17*−*26*) have designed peptidic inhibitors of fibrillogenesis, targeted to highly amyloidogenic regions of Aβ1−40, either $K^{16}LVFFAE^{22}$ of the N-terminal β-sheet (*14*−*25*) or $V^{36}GGVV^{40}$ of the C-terminal β-sheet (*26*). Our inhibitors have *N*-methyl amino acids or esters at alternate positions in the amyloidogenic region $K^{16}LVFFAE^{22}$. *N*-Methyl amino acids, in particular, force the sequence into an extended conformation (*15*), with one normal hydrogen bonding "face" and a second "face" in which the *N*-methyl groups interfere with hydrogen bonding. In line with this strategy, we will describe two peptides, called 2NMe(NTerm) and 2NMe(CTerm), that were designed to prevent aggregation at only one of the two hydrophobic domains of Aβ1−40, while leaving the other unperturbed, and still potentially able to form β-sheet fibrils. We will present evidence that disruption of each of the two β-sheets, one at a time, still allows the disrupted Aβ1−40 molecule to form fibrils, though with different morphology and fibrillogenesis kinetics from those of Aβ1−40. As a further test of the structural double β-sheet model, we also will describe the synthesis and characterization of a congener of Aβ1−40 containing four *N*-methyl groups, 4NMe, in which both of these hydrophobic domains are targeted by the incorporation of *N*-methyl amino acids. We will show that disrupting both of these domains completely eliminates formation of fibrils by this Aβ1−40 congener.

MATERIALS AND METHODS

Peptide Synthesis and Purification. Aβ1−40 (NH_2-DAEFRHDSGY[10] EVHHQKLVFF[20] AEDVGSNKGA[30] IIGLMVGGVV[40]-COOH) was synthesized using modified 9-fluorenylmethoxycarbonyl (FMOC) and HBTU/HOBT (Fastmoc) chemistry on an Applied Biosystems (Foster City, CA) model 433A instrument. Peptides were cleaved from the resin using 9 mL of TFA plus 0.5 mL of thioanisole, 0.3 mL of ethanedithiol, and 0.2 mL of anisole for 1.5 h at 22 °C. Peptides were purified by reverse-phase HPLC using a preparative C18 (Zorbax) column at 60 °C. Peptide purity was greater than 98% by analytical HPLC. The molecular mass of the peptide was verified by ESI- and MALDI-TOF mass spectrometry.

The *N*-methylated peptides were synthesized as described above, except that the residues immediately following the *N*-methyl amino acids (Fmoc-NMe-Phe(OH), Fmoc-Sar (OH) (equivalent to Fmoc-NMe-Gly(OH)), and Fmoc-NMe-Val(OH) from Peptides International, and Fmoc-NMe-Leu from Anaspec) were coupled manually overnight using HATU as the coupling agent.

Kinetics of Fibrillogenesis. The purified Aβ peptides were stored as follows. Peptide was dissolved at ≈50 °C into 30:70 acetonitrile:water (v/v) containing 0.1% TFA (v/v), lyophilized as aliquots of 0.5 mg in siliconized 1.5 mL tubes, and stored at −20 °C.

One goal in these studies was to compare peptides containing *N*-methyl amino acids in both of the two hydrophobic regions believed to be critical for fibril formation (4NMe), with those peptides containing *N*-methyl amino acids in only one of these regions (2NMe(NTerm) and 2NMe(CTerm)). In addition, we will show below that the congener of Aβ1−40 containing four *N*-methyl groups (4NMe) maintains its monomeric state even at concentrations exceeding 1 mM, making it suitable for future detailed structural studies using NMR techniques. For both of these reasons, fibril morphology and fibrillogenesis kinetics were assessed twice: once using a disaggregation procedure that has become standard in our laboratory, and once not using this procedure. By using conditions that do not disaggregate seed nuclei completely, we hoped to give a rigorous test to the ability of *N*-methyl amino acids to prevent aggregation of peptides into fibrils.

For those experiments in which peptides were disaggregated before measurement of fibrillogenesis kinetics, we implemented the procedure derived from previous studies (*11*), in which we compared numerous methods for disaggregating Aβ1−40. In those studies, we observed that initial solubilization of the peptide in DMSO gave reproducible fibril kinetics and most closely approximated "seed-free" conditions. Accordingly, the peptides were initially solubilized in neat DMSO at ≈5.8 mM and then rapidly diluted into 10 mM sodium phosphate, pH 7.40 (with 0.02% NaN_3, w/v), to yield a final peptide concentration of ≈100 μM. In all cases, final DMSO concentration was 2% (v/v). Under these conditions of solubilization, oxidation of Met35 was not observed by mass spectrometry.

In other experiments, we dissolved lyophilized peptide directly into buffer, without the usual first step of incubating it in a solvent that would disaggregate seed nuclei (e.g., DMSO). For fibrillogenesis assays, 1 mL of 10 mM sodium phosphate, pH 7.40 + 0.02% NaN_3, was added to each siliconized tube to solubilize the peptide.

Using either solubilization procedure, fibrillogenesis was monitored discontinuously by measuring thioflavin T fluorescence at 37 °C as described (*27*). Briefly, at various times, 10 μL aliquots were taken and diluted into 1 mL of 10 μM thioflavin T solution in 10 mM sodium phosphate, pH 7.40. The sample was pipetted vigorously, and fluorescence was monitored. Measurements (λ_{EX} = 446 nm, λ_{EM} = 490 nm) were made using a Hitachi F-2000 fluorescence spectrophotometer and, after a 3 s delay, were averaged for 10 s using a bandwidth of 10 nm and a photomultiplier voltage of 700 V. In addition, fibrillogenesis was monitored by turbidity, following absorbance of the sample at 450 nm using a Hitachi U-2000 spectrophotometer, in a 1 cm path length cuvette. Peptide concentrations were assessed from absorbance at 274.6 nm (ϵ for Tyr = 1420 M^{-1} cm^{-1}). Because the latter of these two methods of solubilizing peptides does

not give "seed-free" conditions, estimates of peptide concentration by this method are somewhat approximate, since aggregates can contribute to absorbance through light scattering.

Electron Microscopy. Five microliter aliquots of fibril reaction mixtures of Aβ1−40 or NMe peptides were applied to a glow-discharged, 1−400-mesh, carbon-coated support film, washed with water, and stained with 1% uranyl acetate for 30 s. Micrographs were recorded using a FEI Tecnai F30 electron microscope at magnifications of 15000× and 98000×. In addition, the CCD camera added a 1.4× magnification of all images.

Size Exclusion Chromatography. Prior to fibrillogenesis assays, 100 μL of peptide sample (at various concentrations and times, as described in Results) was subjected to size exclusion chromatography using a Superdex 75 column (Amersham) equilibrated with 10 mM sodium phosphate, pH 7.40; the flow rate was 0.5 mL/min. The elution position of the single peak was consistent with that of a monomer the large peak eluting at approximately 41 min is NaN_3.

Analytical Ultracentrifugation. Equilibrium sedimentation experiments were performed using a Beckman Optima XLA ultracentrifuge equipped with an An-60Ti rotor with aluminum two-sector cells. 4NMe was dissolved in 10 mM phosphate buffer, pH 7.40 and dialyzed against this buffer overnight. The final peptide concentration (510 μM) after dialysis was assessed from absorbance at 274.6 nm, using the extinction coefficient for tyrosine of 1420 M^{-1} cm^{-1}. The dialysis buffer was used as the reference buffer. Sedimentation was followed at 275 nm, at 20 °C for 50 h; rotor speed was 50 000 rpm. Equilibrium was demonstrated by the absence of change in profile absorbance for the last ≈275 scans (Figure 7C) taken over the course of approximately 14 h. A plot of ln(absorbance) vs radius^2 yielded a straight line with the equation $Y = 0.574X - 27.65$. From the slope, the molecular weight was calculated using the equation

$$M = \frac{(\text{slope} \times 2RT)}{\omega^2(1 - \bar{v}\rho)}$$

where M = weight average molecular weight, ω = rotor speed (radians s^{-1}), R = gas constant = 8.3×10^7 erg mol^{-1} K^{-1}, T = K, $\bar{v}$ = partial specific volume (cm^3 g^{-1}), and ρ = solvent density (g cm^{-3}). The partial specific volume for this peptide was taken to be 0.734 cm^3 g^{-1}, i.e., that of Aβ1−40 without *N*-methyl amino acids, and solvent density was assumed to be 1 g cm^{-3}.

DPH Fluorescence. "Critical micelle concentration" was estimated using DPH fluorescence (*28*). Fluorescence measurements were performed using a Hitachi F-2000 fluorescence spectrophotometer. Peptide samples were dissolved directly in buffer, and concentrations assessed from absorbance at 274.6 nm as described above. A stock of 200 μM 1,6-diphenyl-1,3,5-hexatriene (DPH, Molecular Probes) in tetrahydrofuran (THF) was prepared, and 7.5 μL of this stock solution was added to 300 μL of the peptide samples. The samples were kept unsealed to allow evaporation of the THF, but were protected from light by aluminum foil to prevent photobleaching of the DPH. After 5 min of incubation (previous experimentation showed that this time was sufficient to obtain maximum fluorescence), fluorescence of the sample was measured (λ_{EX} = 358 nm, λ_{EM} = 430 nm).

Circular Dichroic Spectroscopy. Circular dichroic (CD) spectra were recorded using an AVIV spectropolarimeter. Peptides were dissolved directly in 10 mM phosphate buffer, pH 7.40 at ≈100 μM. Peptide concentration was confirmed by absorbance at 274.6 nm, as described above. A 1 mm path length was used for measurements. Two to three scans were acquired for each peptide from 260 to 190 nm at 1 nm increments. Signals were averaged for 0.5 s. Bandwidth was 1 nm. The cell was maintained at 25 °C. For time course experiments, two scans were acquired for each peptide at intervals of ≈1 day for days 1−6, and two final scans on day 10.

Dityrosine Fluorescence. The possible presence of dityrosine in Aβ1−40 or 4NMe after prolonged (≥15 days) incubation at 37 °C was assayed by fluorescence, essentially as described elsewhere (*50*−*52*). Briefly, peptides were dissolved in 10 mM sodium phosphate, 0.02% NaN_3, pH 7.40, either directly or after first being disaggregated by being dissolved in DMSO (final DMSO concentration ≤2%, v/v). Measurements (λ_{EX} = 300 nm, λ_{EM} = 350−500 nm) were taken on a Hitachi F-2000 fluorescence spectrophotometer with a bandpass of 10 nm, and photomultiplier voltage of 700 V at 240 nm/min.

PICUP (Photoinducible Cross-Linking of Unmodified Proteins). This procedure was essentially as described by Fancy and Kodadek (*43*, *46*), as modified by Bitan and Teplow (*44*) and Vollers, Teplow, and Bitan (*45*). For the PICUP reaction, 36 μL of Aβ1−40 or 4NMe at 2 mg/mL (462 μM) was mixed with 2 μL of 1 mM (ruthenium(II) tris-bipyridyl dication ($Ru(II)bpy_3^{2+}$)) and 2 μL of 20 mm ammonium persulfate (APS) in a 750 μL Eppendorf tube. The sample was excited at "0nm" on a Hitachi F2000 fluorescence spectrophotometer for 30 s. The sample was then quenched by the addition of 10 μL of 3× sample buffer (12% SDS, 36% glycerol, 150 mM Tris, 6% mercaptoethanol, 0.03% Serva Blue, pH 6.80). 30 μL of the resulting solution was then loaded onto a precast 16.5% T/6% C gel (BioRad). Gel electrophoresis was performed according to the procedure of Schägger and von Jagow (*53*).

RESULTS

Design and Synthesis of the Peptides. *N*-Methyl amino acids were employed as "probes" to disrupt hydrogen bonding in only one of the two putative β-sheets of Aβ1−40, while leaving the other domain covalently unmodified. As described above, solid-state NMR studies indicate that each molecule of Aβ1−40 in fibrils is part of two spatially separate β-sheets, residues 12−24 and 30−40. Studies in our laboratory have shown that the *N*-methyl amino acids disrupt β-sheet aggregation, even while preserving the extended conformation of the polypeptide chain (ref *15*; see also refs *29*−*34*). The replacement of the amide hydrogen by a methyl group interferes with hydrogen bonding that is necessary for propagation of the β-sheet in fibrils. In addition, our fibrillogenesis inhibitors containing *N*-methyl amino acids at alternate residues had solubility properties that are useful for our present purposes; in particular, they are surprisingly water soluble, much more so than nonmethylated peptides of the same sequence. For example, while Ac-

KLVFF-$CONH_2$, a peptide based on the amyloidogenic hydrophobic core domain of Aβ (residues 16−20), readily forms fibrils, the N-methylated analogue of this peptide, Ac-KmeLVmeFF-$CONH_2$ (meL = *N*-methyl-Leu, meF = *N*-methyl-Phe), does not form fibrils, inhibits fibril formation by Aβ1−40, and is water soluble at concentrations above 30 mM (*14*, *15*). For these reasons, we chose incorporation of *N*-methyl amino acids as our method for disrupting aggregation in each of the β-sheet regions of Aβ1−40 while maintaining most of the secondary structural features of the peptide. We synthesized three peptides: 2NMe(NTerm) with *N*-methyl amino acids at positions Leu17 and Phe19, 2NMe-(CTerm) with *N*-methyl amino acids at Gly37 and Val39, and 4NMe with *N*-methyl amino acids at all four positions, Leu17, Phe19, Gly37, Val39.

2NMe Aβ1−40 Congeners Aggregate More Slowly Than Aβ1−40. As described in Materials and Methods, we tested in two different ways whether the Aβ1−40 peptides containing either two (2NMe(NTerm) and 2NMe(CTerm)) or four (4NMe) *N*-methyl amino acids formed fibrils: once with a disaggregation procedure to approximate "seed-free" conditions, and once without such a procedure. Our usual procedure for removing preformed seed nuclei is to dissolve the peptide as a stock in neat DMSO, followed by dilution of the peptide into buffer, as described elsewhere (*11*). In other experiments, we did not use any of the common methods for disrupting initial aggregates; for this set of experiments, the lyophilized peptides were dissolved directly into 10 mM sodium phosphate, pH 7.40 and incubated at 37 °C under quiescent conditions. In both types of experiments, the extent of aggregation was followed by both thioflavin T fluorescence and turbidity (monitoring absorbance at 450 nm) measurements. Because of the concern that some of the modified Aβ peptides might not bind thioflavin to the same extent as unmodified Aβ1−40, we also measured turbidity. In addition, we generally confirmed aggregation by performing electron microscopy when thioflavin T and/or turbidity measurements indicated that the fibrillization reaction was at an end.

2N Methyl Aβ1−40 Peptides Aggregate into Fibrils More Slowly Than Unmodified Aβ1−40, Even in the Absence of an Initial Disaggregation Procedure. We observed that both of the 2NMe peptides were capable of aggregating into fibrils, but more slowly than Aβ1−40. In addition, as shown in Figure 1, electron micrographs reveal morphological differences among fibrils made by these peptides. In Figure 1, the electron micrographs in column 1 show fibrils formed without an initial disaggregation procedure. Figure 1A shows fibrils of unmodified Aβ1−40. 2NMe(NTerm) formed fibrils (Figure 1D), but electron microscopy revealed that the precipitates also contained amorphous material that appeared to coat the edges of the fibrils, i.e., a fibrillar core with unfibrillized material along the edges of the fibril. In addition, there were a large number of spherical particles with a mean diameter of 9.48 nm ± 1.43 nm. In contrast, as shown in Figure 1G, 2NMe(CTerm) appeared more uniformly fibrillized, and the fibrils were highly twisted compared with either Aβ1−40 or 2NMe(NTerm). The two 2NMe peptides also differed slightly in diameter. 2NMe(NTerm) formed fibrils with D = 9.35 ± 0.92 nm, while 2NMe(CTerm) formed fibrils with D =11.23 ± 1.18 nm. These values flanked the value obtained for Aβ1−40 fibrils, with D = 10.88 ± 1.5 nm.

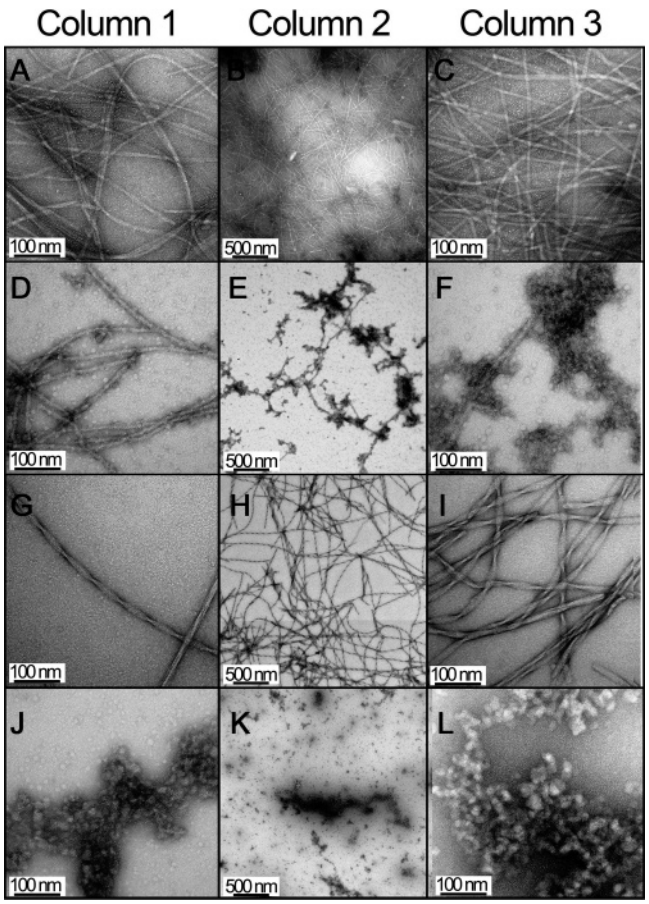

FIGURE 1: Electron micrographs of fibrils/precipitates. Figures in column 1 are electron micrographs of fibrils or precipitates formed after peptides are dissolved directly into buffer. Figures in columns 2 and 3 are electron micrographs of precipitates formed by dissolving peptides in buffer after a disaggregation procedure. Precipitates are negatively stained, bar = 100 or 500 nm, as indicated. (A, B, C) Aβ1−40 fibrils showed typical fibril morphology and had a mean diameter of 10.88 ± 1.50 nm. Magnifications are 98000×, 15000×, and 98000×, respectively. (D, E, F) 2NMe-(NTerm) showed fibrils that appear to be coated with fuzzy edges of amorphous aggregate; in addition, there are numerous spherical particles. Mean diameter of the fibril was 9.35 ± 0.92 nm. Magnifications are 98000×, 15000×, and 98000×, respectively. (G, H, I) 2NMe(CTerm) exhibited abundant very long, and highly and uniformly twisted fibrils with a mean diameter of 11.23 ± 1.18 nm. Magnifications are 98000×, 15000×, and 98000×, respectively. (J, K, L) 4NMe exhibited amorphous deposits only after prolonged incubation (>2 weeks). Magnifications are 98000×, 15000×, and 98000×, respectively. In all cases, the appearance of the fibrils or precipitates is qualitatively similar to those formed without the disaggregation procedure. In addition, fibril diameters are the same within experimental limits.

Fibrils of both of the 2NMe peptides gave rise to thioflavin fluorescence (Figure 2A and Table 1). Data were analyzed using a stretched exponential equation (*11*),

$$\mathrm{ThT} = \mathrm{ThT}_0 + \{(\mathrm{ThT}_\infty - \mathrm{ThT}_0)[1 - \exp(-(kt)^n)]\} \quad (1)$$

where ThT, ThT_0, and ThT_∞ represent thioflavin fluorescence readings at various times, at time = 0, and at infinite time, respectively. Because there had been no disaggregation procedure in these experiments, there was generally little or

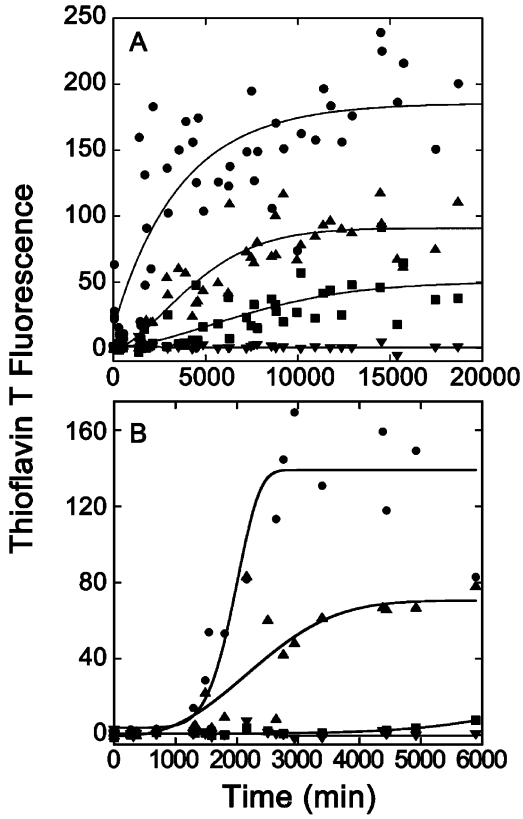

FIGURE 2: (A) Fibrillogenesis kinetics for peptides dissolved in buffer without an initial disaggregation procedure, as monitored by thioflavin T fluorescence: Fibril kinetic growth curves of Aβ1−40 (●), 2NMe(NTerm) (■), 2NMe(CTerm) (▲), and 4NMe (▼) as a function of thioflavin T fluorescence. Peptides ($\approx$100 μM) were incubated at 37 °C in 10 mM sodium phosphate, pH 7.40, also containing 0.02% NaN_3. Data were fitted to a stretched exponential equation $ThT = ThT_0 + (ThT_\infty - ThT_0)[1 - \exp(-(kt)^n]$, where ThT, ThT_0, and ThT_∞ represent thioflavin fluorescence readings at various times, at time = 0, and at infinite time, respectively. (B) Fibrillogenesis kinetics for peptides dissolved in buffer after an initial disaggregation procedure, as monitored by thioflavin T fluorescence: Fibrillogenesis kinetics curves for Aβ1−40 (●), 2NMe(NTerm) (■), 2NMe(CTerm) (▲), and 4NMe (▼) disaggregated by DMSO as measured using thioflavin T fluorescence. Conditions for fibrillogenesis are otherwise as above. Data accumulated from four experiments were fitted to the same equation as above.

Table 1

peptide	fibril diameter, nm	k, min^{-1} without disaggregation	k, min^{-1} with disaggregation
Aβ1−40	10.88 ± 1.50	5.08×10^{-4}	4.85×10^{-4}
2NMe(NTerm)	9.35 ± 0.92	1.61×10^{-4}	8.88×10^{-5}
2NMe(CTerm)	11.23 ± 1.18	2.20×10^{-4}	3.45×10^{-4}

no lag period, and these kinetics were indistinguishable from monoexponential kinetics:

$$ThT = ThT_0 + \{(ThT_\infty - ThT_0)[1 - \exp(-kt)]\} \quad (2)$$

The calculated rates constants were as follows: NMe-(NTerm), $k = 1.61 \times 10^{-4}$ min^{-1} ($\pm$ 1.68×10^{-5} min^{-1}); 2NMe(CTerm), $k = 2.20 \times 10^{-4}$ min^{-1} ($\pm$ 3.31×10^{-5} min^{-1}) compared to that of Aβ1−40, $k = 5.08 \times 10^{-4}$ min^{-1} ($\pm$ 5.76×10^{-5} min^{-1}). Because these assays had been performed in the absence of a disaggregation procedure, the rates were somewhat variable from sample to sample. Nevertheless, the results shown in Figure 2 were typical of those obtained in replicate samples, and suggested that disruption of either one of the β-sheet regions by incorporation of *N*-methyl amino acids slowed fibril formation compared with Aβ1−40, but still allowed fibrils to form. Despite the morphological differences between 2NMe-(NTerm) and 2NMe(CTerm) fibrils, both peptides formed fibrils at similar rates, which were about half that Aβ1−40 itself.

Fibrillogenesis Kinetics of 2NMe Peptides Dissolved after an Initial Disaggregation Procedure To Remove Preformed Seed Nuclei. To compare fibrillogenesis kinetics of these peptides in the absence of preformed seed nuclei, we also measured kinetics after first disaggregating the peptides using the conditions previously found to render Aβ1−40 monomeric (*11*), i.e., initially dissolving the peptides in DMSO followed by diluting them with 10 mM sodium phosphate, pH 7.40 to a final DMSO concentration of $\approx$2%. Electron micrographs of fibrils (or amorphous precipitate, in the case of 4NMe) formed after the disaggregation procedure were qualitatively similar to those formed with a disaggregation procedure (columns 2 and 3 of Figure 1). Kinetics were analyzed using eq 1, i.e., the stretched exponential equation (Figure 2B and Table 1). From this analysis, we obtained the following values for rate constants: for Aβ1−40, $k = 4.85 \times 10^{-4}$ min^{-1} ($\pm$ 3.24×10^{-5} min^{-1}); for 2NMe-(CTerm), $k = 3.45 \times 10^{-4}$ min^{-1} ($\pm$ 2.88×10^{-5} min^{-1}), but for 2NMe(NTerm), $k = 8.88 \times 10^{-5}$ min^{-1} ($\pm$ 2.20×10^{-5} min^{-1}). Although 2NMe(CTerm) fibrils showed maximal thioflavin T fluorescence about half of that for Aβ1−40 fibrils formed at the same peptide concentration, the rate constants for both Aβ1−40 and 2NMe(CTerm) were similar whether or not the peptides initially underwent disaggregation procedures. In contrast, after a disaggregation procedure, 2NMe(NTerm) formed fibrils at a rate nearly 1 order of magnitude lower than either of the other peptides.

Concentration Dependence of 2NMe(NTerm) Fibrillogenesis Kinetics. Figures 2A and 2B show that both 2NMe peptides attained lower values for final thioflavin T fluorescence than did Aβ1−40. This is especially true for 2NMe-(NTerm), for which the thioflavin T fluorescence barely rises above background levels. We hypothesized, however, that the difference between 2NMe(NTerm) and Aβ1−40 was not a qualitative difference in the kinetics of fibril formation, but simply a matter of the starting peptide concentration needed to sustain a fibrillogenesis reaction. Figure 3A shows fibrillogenesis kinetics for 2NMe(NTerm) at four different concentrations from 50 to 400 μM (fibrillization measured without an initial disaggregation procedure). At concentrations of 100−400 μM, the peptide formed fibrils, while at 50 μM, the peptide did not form fibrils by the criterion of thioflavin T fluorescence. Figure 3B shows that the value calculated for ThT_∞ using eq 1 was proportionate to peptide concentration, while the rate constant remained unchanged.

Formation of Micelle-like Aggregates by 2NMe(NTerm) and 2NMe(CTerm). Diphenylhexatriene (DPH) fluorescence was used to measure aggregation of 2NMe peptides into micelle-like aggregations. In agreement with Soreghan et al. (*35*) and our previous measurements (*36*), Aβ1−40 showed a "critical micelle concentration" ("CMC") of $\approx$50 μM (Figure 4). 2NMe(NTerm) and 2NMe(CTerm) showed

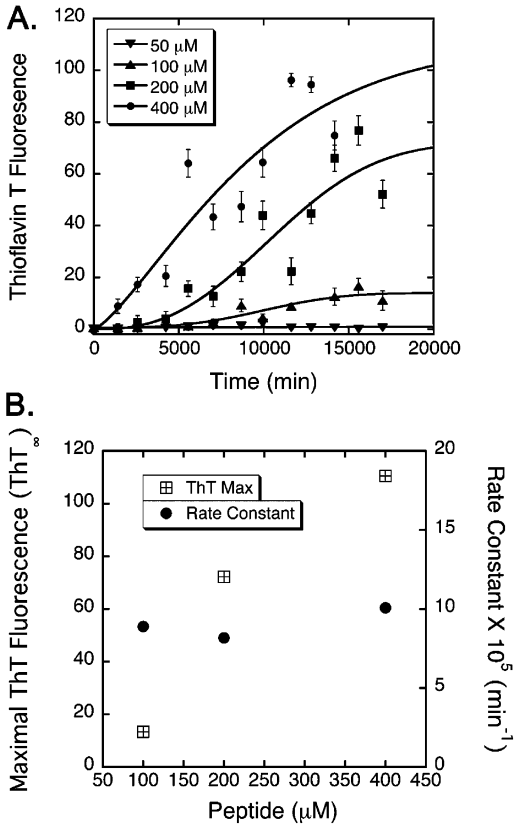

FIGURE 3: Fibrillogenesis kinetics of 2NMe(NTerm) as a function of initial peptide concentration: (A) 2NMe(NTerm) was initially disaggregated using DMSO, and then diluted into 10 mM sodium phosphate, pH 7.40 to final concentrations of 50, 100, 200, or 400 μM. Experimental conditions and methods of analysis were as described for Figure 2. Data were analyzed using the equation of a stretch exponential, eq 1. (B) The figure shows the rate constant, k, and thioflavin fluorescence at infinite time, ThT_∞, as a function of initial peptide concentration.

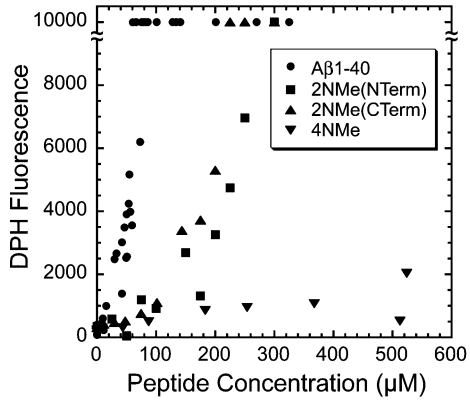

FIGURE 4: Micelle formation of Aβ1−40, 2NMe(NTerm), and 2NMe(CTerm): Diphenylhexatriene (DPH) fluorescence was used to monitor micelle formation. The following were obtained for CMCs: Aβ1−40, ≈50 μM (●); 2NMe(NTerm), ≈200 μM (■); 2NMe(CTerm), ≈200 μM (▲), and 4NMe (▼) exhibited no micelles. Fluorescence that reached the maximum of the fluorometer appears as a plateau in the signal.

similar "CMCs" (Figure 4), in both cases ≈200 μM, somewhat higher than that of Aβ1−40. The fact that both the 2NMe(NTerm) and 2NMe(CTerm) have similar "CMCs" suggests that both the N and C terminal regions contribute to micelle formation, since in each case, either the N-terminal or the C-terminal is altered by *N*-methyl amino acids.

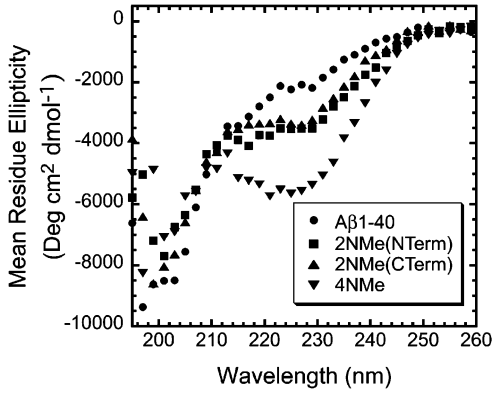

FIGURE 5: Circular dichroism of Aβ1−40, 2NMe(NTerm), and 2NMe(CTerm): CD spectra of freshly dissolved peptide samples at ≈100 μM in 10 mM phosphate buffer, pH 7.40. Samples were scanned in a 1 mm cuvette from 290 nm to 190 nm at 37 °C for Aβ1−40 (●), 2NMe(NTerm) (■), 2NMe(CTerm) (▲), and 4NMe (▼). The scan was in 1 nm increments, and data were averaged for 1 s. Because of high CD dynode values below 195 nm, the spectra could be measured ≥195 nm.

Circular Dichroic Spectra of 2NMe(NTerm) and 2NMe-(CTerm). Previous studies of fibrillogenesis inhibitor peptides containing *N*-methyl amino acids showed CD spectra consistent with a β-strand conformation, but there is a markedly red-shifted, single minimum at 225−226 nm (*15*). NMR studies also were consistent with a β-strand conformation (*15*). Figure 5 shows the CD spectra of freshly dissolved 2NMe(NTerm) and 2NMe(CTerm), and of unmodified Aβ1−40. (The spectrum of 4NMe is also shown, and is discussed below.) The spectrum of Aβ1−40 was consistent with mainly "random coil" conformation, as previously described (*37*−*40*). The spectra of the two 2NMe peptides were similar to each other, and were similar to that of Aβ1−40, except that an additional minimum was observed at 225 nm, as observed previously for other *N*-methyl amino acid containing peptides (*14*, *15*). The spectrum for 4NMe was similar to that of the two 2NMe peptides, except that the trough at 225 nm was approximately twice as deep as that of the two 2NMe peptides, as might be expected since 4NMe has twice the number of *N*-methyl amino acids per molecule. These spectra are consistent with the notion that the *N*-methyl amino acids induce only local structural perturbations. In addition, from previous NMR studies of related *N*-methyl amino acid containing peptides derived from Aβ, we infer that the local conformation around the *N*-methyl amino acids may be extended or β-strand in these peptides, as it is in the inhibitor peptides (*16*).

Figure 6 shows the evolution of the CD spectra of 2NMe-(NTerm) and 2NMe(CTerm) over time. Despite similar initial CD spectra and similar "CMCs", the evolution of the spectra of the two 2NMe peptides differ considerably. The CD spectrum of 2NMe(NTerm) at ≈100 μM changes little over this time period. This lack of change is consistent with the data in Figure 2, showing that, at this concentration, the thioflavin T fluorescence rises only slightly above the background level. In contrast, the CD spectrum of 2NMe-(CTerm) evolves, and diverges from that of 2NMe(NTerm) starting around day 4. 2NMe(CTerm) shows an increasing positive peak with a maximum at ≈200 nm, and an increasing trough with a minimum at ≈219 nm. These changes are consistent with the development of increasing

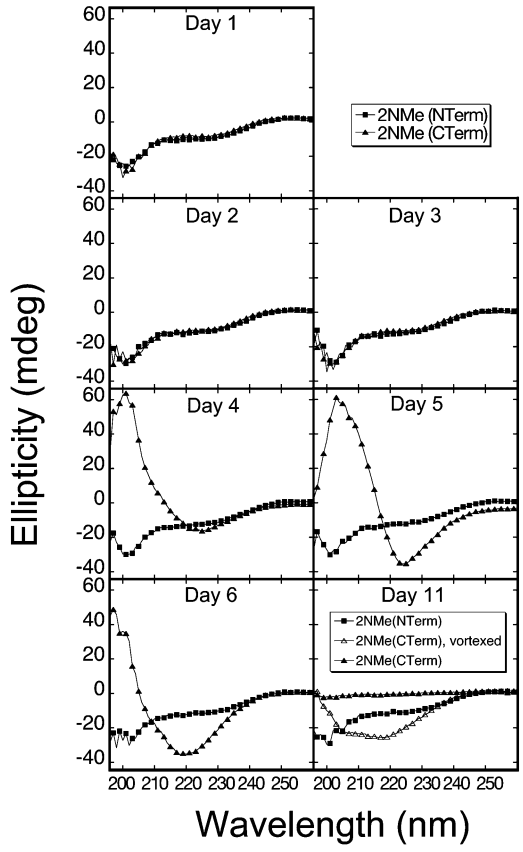

FIGURE 6: Evolution of CD spectra of 2NMe(NTerm) and 2NMe-(CTerm) over the course of an 11 day period: CD spectra of peptides at ≈100 μM in 10 mM phosphate buffer, pH 7.40, comparing 2NMe(NTerm) (●) and 2NMe(CTerm) (▲). Most of the spectra show samples that were neither centrifuged nor vortexed. For the sample of 2NMe(CTerm) on day 11, however, most of the signal had disappeared because of the formation of precipitate; therefore, spectra are shown for the sample both with (△) and without (▲) vortexing.

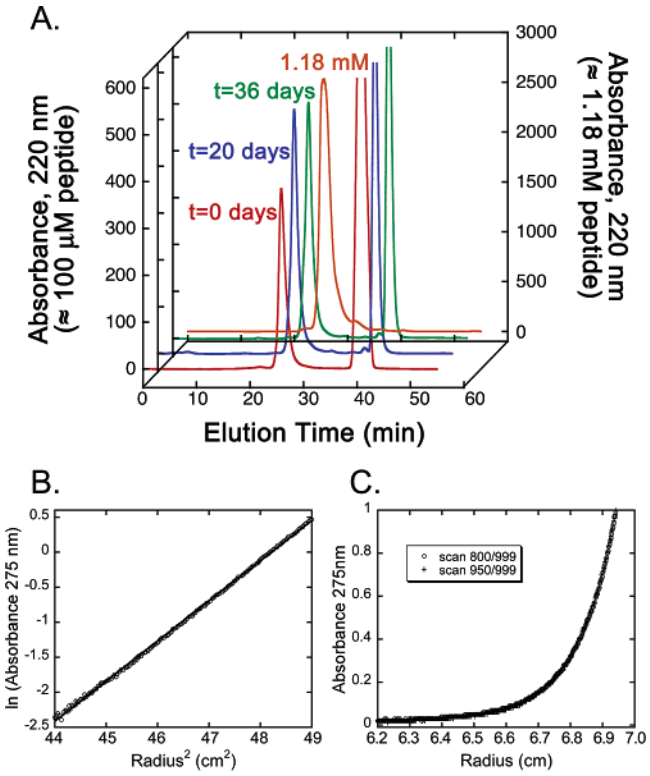

FIGURE 7: (A) Size exclusion chromatography of 4NMe: 100 μL of a solution of 4NMe at an initial peptide concentration of 1.18 mM (orange line) was chromatographed using a Superdex 75 size exclusion column. A single peak eluting at ≈26 min, corresponding to a monomeric molecular weight, was observed. In addition, a solution of 4NMe at ≈100 μM was incubated for five weeks, and at various intervals (red line, 0 days; blue line, 20 days; and green line, 36 days) was chromatographed using the same column. The single peptide peak corresponds to a monomeric molecular weight; the large peak at ≈41 min is NaN_3. (B, C) Sedimentation equilibrium analytical ultracentrifugation of 4NMe: (B) 4NMe was dissolved in 10 mM phosphate buffer, pH 7.40 and dialyzed against this buffer overnight. The final peptide concentration (510 μM) after dialysis was assessed from absorbance at 274.6 nm, using the extinction coefficient for tyrosine of 1420 M^{-1} cm^{-1}. The dialysis buffer was used as the reference buffer. Sedimentation was followed at 275 nm, at 20 °C for 50 h; rotor speed was 50 000 rpm. From the slope of ln(absorbance 275 nm) as a function of radius^2 (from the center of rotation), an apparent weight-average molecular weight, *M*, of 3830 Da was calculated. (C) Equilibrium was demonstrated by the absence of change in profile absorbance for the last ≈275 scans taken over the course of approximately 14 h (scans 800 and 950 are shown and are superimposable).

β-sheet content by 2NMe(CTerm) over this time period, and are consistent with the fibril formation observed by ThT fluorescence.

4NMe Maintains a Monomeric State Indefinitely, Even at Concentrations >1 mM. Figures 2A and 2B, in addition to showing the time course of thioflavin T fluorescence for Aβ1−40, 2NMe(NTerm), and 2NMe(CTerm), also show that 4NMe does not self-associate into thioflavin T positive aggregates, whether or not an initial disaggregation procedure is used. At concentrations up to >600 μM, 4NMe does not induce DPH fluorescence (Figure 4), and thus does not make micelle-like aggregates at these concentrations.

Figure 7A shows size exclusion chromatography of 4NMe using a Superdex 75 column. At concentrations up to 1.18 mM, the peptide eluted in a single peak, the elution time of which, ≈26 min, was consistent with a monomeric molecular weight. In addition, repeated size exclusion chromatography of a 4NMe sample incubated at 37 °C for over five weeks showed only the same peak of monomeric peptide. Figures 7B and 7C show sedimentation equilibrium analytical ultracentrifugation of 4NMe (≈510 μM, 50 000 rpm, 20 °C). The results indicated a single species with a molecular weight of 3830 Da, close to the expected monomer molecular weight of 4385 Da. The slightly low value of the apparent molecular weight has been observed for other peptides containing *N*-methyl amino acids (*14*, *15*), and this nonideal behavior may be attributable to rigidity of the peptide backbone in the region of the *N*-methyl amino acids. Finally, Figure 8 shows CD spectra of 4NMe at ≈100 μM over a time course of 11 days, i.e., similar to the time period shown for Aβ1−40, 2NMe(NTerm), and 2NMe(CTerm) in Figure 6. Over this time, the CD spectrum of 4NMe did not change, indicating that the conformation of the peptide remained stable, and supporting the notion that 4NMe did not self-associate.

The above data all indicate that this peptide does not self-associate at all, and maintains a monomeric state at all concentrations up to at least 1.18 mM.

Dityrosine Formation and Tyrosine Exposure in 4NMe. After prolonged incubation of 4NMe (>2 weeks) at 37 °C, a small amount of precipitate formed. As shown in Figures

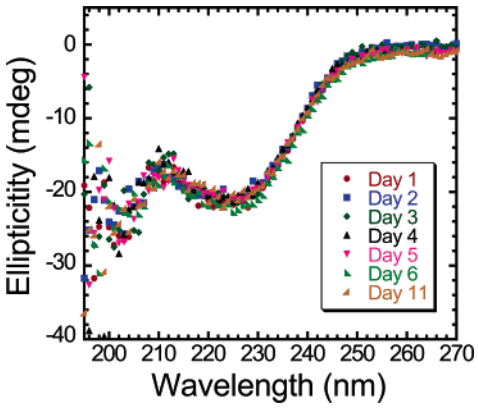

FIGURE 8: Circular dichroism time course of 4NMe. Peptide was dissolved at ≈100 μM in 10 mM sodium phosphate buffer, pH 7.40 and incubated under quiescent conditions at 37 °C. At various times, the CD spectrum of peptide in a 1 mm cuvette was measured from 270 to 190 nm, with 1 nm increments, and signal averaging for 0.5 s.

1J, 1K, and 1L, this precipitate was not fibrillar, which is consistent with the absence of thioflavin T positivity in this material (Figures 2A and 2B). We hypothesized that this small amount of precipitate could be attributed to formation of intermolecular dityrosine cross-links between the sole Tyr residues (Tyr^{10}) of peptide molecules. Formation of dityrosine has been reported for Aβ1−40 (*41*, *42*), and could occur to an even greater extent in the highly soluble 4NMe peptide than in Aβ1−40. Figure 9A shows fluorescence spectra (λ_{EX} = 300 nm, λ_{EM} = 350−500 nm) for both the Aβ1−40 and 4NMe precipitates after 15 days, compared to freshly solubilized 4NMe. The soluble Aβ1−40 showed only background signal in this wavelength range. Aβ1−40 precipitates, which had formed over 15 days, showed an increase in apparent fluorescence due to light scattering by fibrils, and in addition showed a small peak at ≈410 nm, consistent with the presence of dityrosine cross-links. In contrast, 4NMe, with little precipitate, showed a large peak at ≈410 nm, again consistent with dityrosine cross-links, and showed only a small scattering effect from its sparse aggregates. No difference was seen between samples initially treated with DMSO and those dissolved directly into buffer (data not shown).

The fact that 4NMe was more prone to dityrosine formation than Aβ1−40 suggests that Tyr10 was more accessible to free radical formation in 4NMe than in Aβ1−40. To test this hypothesis, we performed PICUP (photoinducible cross-linking of unmodified protein) assays (*43*−*45*) on solutions of 4NMe and Aβ1−40, both at a concentration of 2 mg/mL (462 μM). PICUP cross-links peptides through light-induced one-electron transfers that generate radicals, mainly tyrosyl radicals (*46*). As expected for a monomeric and highly soluble protein (*44*, *45*, *48*, *49*) (Figure 9B), random association of 4NMe led to the formation of a ladder of bands, with more extensive cross-linking than for Aβ1−40. Since 4NMe is monomeric at this concentration (see Figures 4, 7, and 8), while Aβ1−40 is above its "CMC", the extensive cross-linking of 4NMe is consistent with the idea that the sole Tyr in this peptide is more solvent exposed than in Aβ1−40.

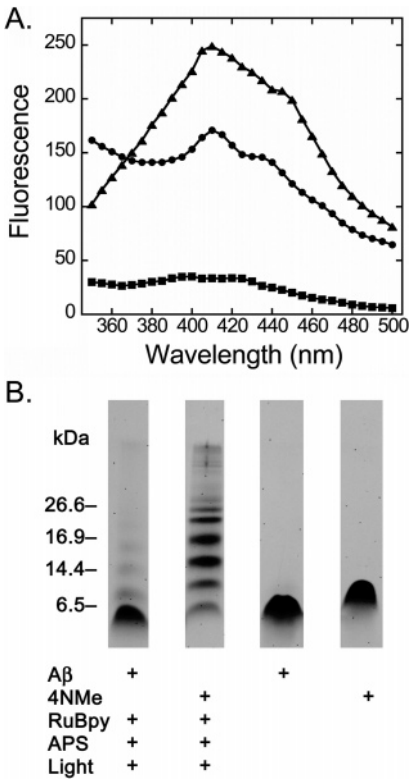

FIGURE 9: (A) Dityrosine formation as monitored by fluorescence. Aβ1−40 or 4NMe incubated at 37 °C for >15 days develops fluorescence, consistent with the formation of intermolecular dityrosine cross-links. Peptides were dissolved in 10 mM sodium phosphate, 0.02% NaN_3, pH 7.40, either directly or after first being disaggregated by being dissolved in DMSO (final DMSO concentration ≤2%, v/v). Measurements (λ_{EX} = 300 nm, λ_{EM} = 350−500 nm) were taken on a Hitachi F-2000 fluorescence spectrophotometer with a bandpass of 10 nm, and PM voltage of 700 V at 240 nm/min. Symbols: (■) fresh Aβ1−40 solution; (●) Aβ1−40 solution incubated at 37 °C for >15 days; (▲) 4NMe incubated at 37 °C for >15 days. (B) PICUP assays of Aβ1−40 and 4NMe: Aβ1−40 (4.3 kDa) and 4NMe at 2 mg/mL (462 μM) were mixed with RuBpy and APS and exposed to light as described in Materials and Methods. Aβ1−40and 4NMe both showed a ladder of oligomeric species, but the cross-linking of the latter peptide was clearly more extensive. Without reagents for the PICUP reaction, both of these peptides had migrations consistent with that of monomers.

DISCUSSION

Our goal was to disrupt each of the two putative β-sheets of Aβ1−40 individually, without disrupting the other. To this end, we used *N*-methyl amino acids to disrupt the hydrogen bonding that stabilizes the sheets. In addition, previous NMR studies suggest that *N*-methyl groups confer an extended, or β-strand conformation locally in peptides, and also greatly increase water solubility when they are incorporated into fibril-forming peptides, such as internal fragments of Aβ (e.g., Ac-KLVFF-NH_2, residues 16−20 of Aβ) or the prion protein (residues 106−129) (*14*, *15*). We were then in a position to ask whether the nonmodified β-sheet could still form when the other β-sheet was disrupted by local incorporation of two *N*-methyl amino acids. Two such modified residues are sufficient to prevent the propagation of hydrogen bonds into a β-sheet, but do not grossly distort the torsional geometry of the β-strands into which they are incorporated (*15*). This approach addresses an emerging model of Aβ1−40 as forming a double molecular

layer of β-sheets connected by a bend in the side-chain dimension (*12*, *13*). In addition, we asked whether disruption of both β-sheet domains is necessary to prevent fibril formation altogether.

Our data indicate that incorporation of *N*-methyl amino acids into a single β-sheet domain of Aβ1−40 does slow fibrillogenesis and alters the morphology of the fibril. Furthermore, disruption of the N- or C-terminal β-sheet domains by *N*-methyl amino acids has strikingly different effects on fibrillogenesis kinetics and fibril morphology. Finally, disruption of both β-sheet domains is necessary to prevent fibril formation.

Although *N*-methyl amino acids in either N- or C-terminal β-sheets interfered with fibril formation, the effect on fibrillogenesis kinetics was much more profound for 2NMe-(NTerm) than 2NMe(CTerm). As summarized in Table 1, whether an initial disaggregating procedure was used or not, both peptides formed fibrils more slowly than Aβ1−40, but the effect was significantly more marked for 2NMe(NTerm) than 2NMe(CTerm). In addition, the final values attained in thioflavin T fluorescence assays (ThT_∞ in eq 1) were lower than that for Aβ1−40 at the same peptide concentration, indicating that both 2NMe peptides have higher "critical concentrations", which we define as the concentration below which fibrils cannot be detected experimentally, than Aβ1−40. This was confirmed for 2NMe(NTerm), by showing that the difference in ThT_∞ values between 2NMe(NTerm) and Aβ1−40 could be mostly eliminated by using higher initial concentrations of peptide to form fibrils (Figure 3).

Electron microscopy and CD spectroscopy revealed striking differences between 2NMe(NTerm) and 2NMe(CTerm). Electron micrographs of 2NMe(NTerm) showed the fibrils to have a slightly narrower diameter than Aβ1−40 fibrils, and to have fuzzy edges along the length of the fibril axis, characteristic of unfibrillized material. In addition, large numbers of spherical aggregates were present. These results are consistent with the proposition that fibrils of this peptide were formed mainly from its C-terminal β-sheet, leaving a large segment of the peptide as unfibrillized material, visible as the fuzzy edge along fibrils. Furthermore, the spherical aggregates may represent either oligomeric seeds or micelle-like aggregates that did not progress to form fibrils. Evolution of CD spectra over 11 days showed little change from the initial spectrum compared to either 2NMe(CTerm) or Aβ1−40, consistent with the view that at the concentrations used for these measurements ($\approx$100 μM), 2NMe(NTerm) formed mainly spherical aggregates and not fibrils, and also consistent with the low values obtained for ThT_∞. In contrast to 2NMe(NTerm), 2NMe(CTerm) showed more modest retardation of fibrillization, and abundant fibrillar material but no spherical aggregates in electron micrographs, and only modestly reduced values for ThT_∞ compared with Aβ1−40. Electron micrographs also showed very regular, but highly twisted fibrils, suggesting that modification of the C-terminal β-sheet may have interfered with the lateral organization of molecules within the fibril that give rise to the overall pitch of the fibril. Also consistent with this proposal is that 2NMe(CTerm) fibrils have a slightly larger diameter than Aβ1−40 fibrils (D = 11.23 ± 1.18 and 10.88 ± 1.5 nm, respectively). Despite these differences, both 2NMe peptides had similar "critical micelle concentrations" of $\approx$200 μM, i.e., approximately 4-fold higher than that of Aβ1−40. Taken together, these findings suggest that disruption of either β-sheet domain of Aβ1−40 inhibits assembly of the peptide into fibrils, and alters the structure of the fibrils, but that the N-terminal β-sheet domain is the more critical domain for fibrillogenesis.

In contrast to the 2NMe peptides, 4NMe remained monomeric at concentrations above 1 mM, and did not form either micelles or fibrils, as shown by size exclusion chromatography, analytical ultracentrifugation, and circular dichroic spectroscopy. A small amount of precipitate formed over the course of weeks, but this was nonfibrillar material. Fluorescence spectra were consistent with formation of dityrosine cross-links between 4NMe molecules, though other cross-links initiated by tyrosine radicals might also have formed. Despite the fact that Aβ1−40 was above its CMC under the conditions used for the PICUP assay, while 4NMe was monomeric, the latter peptide became more cross-linked in the PICUP assay, suggesting that the tyrosine residue of 4NMe may be more solvent exposed than that of Aβ1−40.

The properties of this congener also suggest its utility for examining a related question. We have presented evidence recently suggesting that the "bend region" connecting the two β-sheets is not a passive follower of the β-sheets in the process of fibrillogenesis. On the contrary, we showed that a congener of Aβ1−40 containing a lactam bridge between the side chains of D23 and K28, mimicking the salt bridge that eventually forms in the fibrils, formed fibrils similar to those of unmodified Aβ1−40, but at $\approx$1000-fold faster rate and without a lag period (*11*). These data suggest that formation of the bend region may represent a rate-limiting step in the overall process of fibril formation. By the same token, Lazo et al. (*47*) have shown that residues 21−30 constitute an autonomously folding, protease resistant domain that, even as a monomeric peptide, adopts a structure reminiscent of the bend region of Aβ1−40. However, the high propensity of Aβ1−40 to aggregate and temporal instability of intermediates in the fibrillogenesis pathway severely limit the use of solution NMR and crystallographic techniques for determining intermediate structure. We have shown that the 4NMe peptide mentioned above is a highly soluble and monomeric congener of Aβ1−40 that will be amenable to studies of the structure and dynamics of the bend region in solution using techniques such as NMR.

Finally, *N*-methyl amino acids have been used in the design of inhibitors of fibrillogenesis (*14*, *15*, *23*), but previously, these inhibitors have targeted only one of the two β-sheet domains, in most cases the N-terminal β-sheet. Our results indicate that the most effective inhibition of Aβ1−40 fibrillogenesis may require that inhibitors of fibril formation target both β-sheets rather than only one.

ACKNOWLEDGMENT

We would like to thank Dr. Mohammed Yousef (Biophysical Core), Dr. Robert Josephs (electron microscopy facility), and Drs. Giridher Reddy and Chang-Jin Win (Mass Spectrometry Facilities), at the University of Chicago.

REFERENCES

1. Benzinger, T. L., Gregory, D. M., Burkoth, T. S., Miller-Auer, H., Lynn, D. G., Botto, R, E., and Meredith, S. C. (1998) Propagating structure of Alzheimer's β-amyloid(10-35) is parallel

β-sheet with residues in exact register, *Proc. Natl. Acad. Sci. U.S.A. 95*, 13407−12.
2. Benzinger, T. L., Gregory, D. M., Burkoth, T. S., Miller-Auer, H., Lynn, D. G., Botto, R. E., and Meredith, S. C. (2000) Two-dimensional structure of β-amyloid(10-35) fibrils, *Biochemistry 39*, 3491−9.
3. Antzutkin, O. N., Balbach, J. J., Leapman, R. D., Rizzo, N. W., Reed, J., and Tycko, R. (2000) Multiple quantum solid-state NMR indicates a parallel, not antiparallel, organization of β-sheets in Alzheimer's β-amyloid fibrils, *Proc. Natl. Acad. Sci. U.S.A. 97*, 13045−50.
4. Balbach, J. J., Petkova, A. T., Oyler, N. A., Antzutkin, O. N., Gordon, D. J., Meredith, S. C., and Tycko, R. (2002) Supramolecular structure in full-length Alzheimer's β-amyloid fibrils: evidence for a parallel β-sheet organization from solid-state nuclear magnetic resonance, *Biophys. J. 83*, 1205−16.
5. Petkova, A. T., Ishii, Y., Balbach, J. J., Antzutkin, O. N., Leapman, R. D., Delaglio F., and Tycko, R. (2002) A structural model for Alzheimer's β-amyloid fibrils based on experimental constraints from solid-state NMR, *Proc. Natl. Acad. Sci. U.S.A. 99*, 16742−7.
6. Buchete, N. V., Tycko, R., and Hummer, G. (2005) Molecular dynamics simulations of Alzheimer's β-amyloid protofilaments, *J. Mol. Biol. 353*, 804−21.
7. Petkova, A. T., Yau, W.-M., and Tycko, R. (2006) Experimental Constraints on Quaternary Structure in Alzheimer's β-Amyloid Fibrils, *Biochemistry 45*, 498−512.
8. Antzutkin, O. N., Balbach, J. J., and Tycko, R. (2003) Site-specific identification of non-β-strand conformations in Alzheimer's β-amyloid fibrils by solid-state NMR, *Biophys. J. 84*, 3326−35.
9. Antzutkin, O. N., Leapman, R. D., Balbach, J. J., and Tycko, R. (2002) Supramolecular structural constraints on Alzheimer's β-amyloid fibrils from electron microscopy and solid-state nuclear magnetic resonance, *Biochem 41*, 15436−50.
10. Malinchik, S. B., Inouye, H., Szumowski, K. E., and Kirschner, D. A. (1998) Structural analysis of Alzheimer's β(1-40) amyloid: protofilament assembly of tubular fibrils, *Biophys. J. 74*, 537−45.
11. Sciarretta, K. L., Gordon, D. J., Petkova, A. T., Tycko, R., and Meredith, S. C. (2005) Aβ40-Lactam(D23/K28) models a conformation highly favorable for nucleation of amyloid, *Biochemistry* 44, 6003−14.
12. Lansbury, P. T., Jr., Costa, P. R., Griffiths, J. M., Simon, E. J., Auger, M., Halverson, K. J., Kocisko, D. A., Hendsch, Z. S., Ashburn, T. T., Spencer, R. G., Tidor, B., and Griffin, R. G. (1995) Structural model for the β-amyloid fibril based on interstrand alignment of an antiparallel-sheet comprising a C-terminal peptide, *Nat. Struct. Biol. 2*, 990−8.
13. Balbach, J. J., Ishii, Y., Antzutkin, O. N., Leapman, R. D., Rizzo, N. W., Dyda, F., Reed, J., and Tycko, R. (2000) Amyloid fibril formation by Aβ16-22, a seven-residue fragment of the Alzheimer's β-amyloid peptide, and structural characterization by solid-state NMR, *Biochemistry 39*, 13748−59.
14. Gordon, D. J., Sciarretta, K. L., and Meredith, S. C. (2001) Inhibition of β-amyloid(40) fibrillogenesis and disassembly of β-amyloid(40) fibrils by short β-amyloid congeners containing N-methyl amino acids at alternate residues, *Biochemistry 40*, 8237−45.
15. Gordon, D. J., Tappe, R., and Meredith, S. C. (2002) Design and characterization of a membrane permeable N-methyl amino acid-containing peptide that inhibits Aβ1-40 fibrillogenesis, *J. Pept. Res. 60*, 37−55.
16. Gordon, D. J., and Meredith, S. C. (2003) Probing the role of backbone hydrogen bonding in β-amyloid fibrils with inhibitor peptides containing ester bonds at alternate positions, *Biochemistry 42*, 475−85.
17. Ghanta, J., Shen, C. L., Kiessling, L. L., and Murphy, R. M. (1996) A strategy for designing inhibitors of β-amyloid toxicity, *J. Biol. Chem. 271*, 29525−8.
18. Tjernberg, L. O., Naslund, J., Lindqvist, F., Johansson, J., Karlstrom, A. R., Thyberg, J., Terenius, L., and Nordstedt, C. (1996) Arrest of β-amyloid fibril formation by a pentapeptide ligand, *J. Biol. Chem. 271*, 8545−8.
19. Tjernberg, L. O., Lilliehook, C., Callaway, D. J., Naslund, J., Hahne, S., Thyberg, J., Terenius, L., and Nordstedt, C. (1997) Controlling amyloid β-peptide fibril formation with protease-stable ligands, *J. Biol. Chem. 272*, 12601−5.
20. Soto, C., Kindy, M. S., Baumann, M., and Frangione, B. (1996) Inhibition of Alzheimer's amyloidosis by peptides that prevent β-sheet conformation, *Biochem. Biophys. Res. Commun. 226*, 672−80.
21. Soto, C., Sigurdsson, E. M., Morelli, L., Kumar, R. A., Castano, E. M., and Frangione, B. (1998) β-sheet breaker peptides inhibit fibrillogenesis in a rat brain model of amyloidosis: implications for Alzheimer's therapy, *Nature Med. 4*, 822−6.
22. Soto, C., Saborio, G. P., and Permanne, B. (2000) Inhibiting the conversion of soluble amyloid-beta peptide into abnormally folded amyloidogenic intermediates: relevance for Alzheimer's disease therapy, *Acta Neurol. Scand. Suppl. 176*, 90−5.
23. Hughes, E., Burke, R. M., and Doig, A. J. (2000) Inhibition of toxicity in the β-amyloid peptide fragment β-(25-35) using N-methylated derivatives: a general strategy to prevent amyloid formation, *J. Biol. Chem. 275*, 25109−15.
24. Hetenyi, C., Szabo, Z., Klement, E., Datki, Z., Kortvelyesi, T., Zarandi, M., and Penke, B. (2002) Pentapeptide amides interfere with the aggregation of β-amyloid peptide of Alzheimer's disease, *Biochem. Biophys. Res. Commun. 292*, 931−6.
25. Chalifour, R. J., McLaughlin, R. W., Lavoie, L., Morissette, C., Tremblay, N., Boule, M., Sarazin, P., Stea, D., Lacombe, D., Tremblay, P., and Gervais, F. (2003) Stereoselective interactions of peptide inhibitors with the beta-amyloid peptide, *J. Biol. Chem. 278*, 34874−81.
26. Cruz, M., Tusell, J. M., Grillo-Bosch, D., Albericio, F., Serratosa, J., Rabanal, F., and Giralt, E. (2004) Inhibition of β-amyloid toxicity by short peptides containing N-methyl amino acids, *J. Pept. Res. 63*, 324−8.
27. LeVine., H., 3rd. (1999) Quantification of β-sheet amyloid fibril structures with thioflavin T, *Methods Enzymol. 309*, 274−84.
28. Zhang, X., Jackson, J. K., and Burt, H. M. (1996) Determination of surfactant critical micelle concentration by a novel fluorescence depolarization technique, *J. Biochem. Biophys. Methods 31*, 145−50.
29. Tonelli, A. E. (1970) Conformational Characteristics of L-Proline Oligomers, *J. Am. Chem. Soc. 92*, 6187−90.
30. Tonelli, A. E. (1971) Stability of Cis and Trans Amide Bond Conformations in Polypeptides, *J. Am. Chem. Soc. 93*, 7153−5.
31. Tonelli, A. E. (1974) Conformational Characteristics of Polypeptides Containing Isolated L-proline Residues with Cis-Peptide Bonds, *J. Mol. Biol. 86*, 627−35.
32. Kumar, N. G., Izumiya, N., Miyoshi, M., Sugano, H., and Urry, D. (1975) Conformational and Spectral Analysis of Polypeptide Antibiotic N-Methylleucine Gramicidin-S Dihydrochloride by Nuclear Magnetic-Resonance, *Biochemistry 14*, 2197−207.
33. Patel, D. J., and Tonelli, A. E. (1976) N-Methylleucine Gramicidin-S and (Di-N-Methylleucine) Gramicidin-S Conformations with Cis L-Orn-L−N-MeLeu Peptide Bonds, *Biopolymers 15*, 1623−35.
34. Vitoux, B., Aubry, A., Cung, M. T., and Marraud, M. (1986) N-Methyl Peptides. 7. Conformational Perturbations Induced by N-Methylation of Model Dipeptides, *Int. J. Pept. Protein Res. 27*, 617−32.
35. Soreghan, B., Kosmoski, J., and Glabe, C. (1994) Surfactant properties of Alzheimer's Aβ peptides and the mechanism of amyloid aggregation, *J. Biol. Chem. 269*, 28551−4.
36. Gordon, D. J., Balbach, J. J., Tycko, R., and Meredith, S. C. (2004) Increasing the amphiphilicity of an amyloidogenic peptide changes the β-sheet structure in the fibrils from antiparallel to parallel, *Biophys. J. 86*, 428−34.
37. Lomakin, A., Chung, D. S., Benedek, G. B., Kirschner, D. A., and Teplow, D. B. (1996) On the nucleation and growth of amyloid β-protein fibrils: detection of nuclei and quantitation of rate constants, *Proc. Natl. Acad. Sci. U.S.A. 93*, 1125−9.
38. Ma, K., Clancy, E., Zhang, Y., Ray, D., Wollenberg, K., and Zagorski, M. (1999) Residue-specific pKa measurements of the β-peptide and mechanism of pH-induced amyloid formation, *J. Am. Chem. Soc. 121*, 8698−706.
39. Kirkitadze, M. D., Condron, M. M., and Teplow, D. B. (2001) Identification and characterization of key kinetic intermediates in amyloid β-protein fibrillogenesis, *J. Mol. Biol. 312*, 1103−19.
40. Danielsson, J., Jarvet, J., Damberg, P., and Graslund, A. (2005) The Alzheimer β-peptide shows temperature-dependent transitions between left-handed 3-helix, β-strand and random coil secondary structures, *FEBS J. 272*, 3938−49.
41. Atwood, C. S., Perry, G., Zeng, H., Kato, Y., Jones, W. D., Ling, K. Q., Huang, X., Moir, R. D., Wang, D., Sayre, L. M., Smith,

M. A., Chen, S. G., and Bush, A. I. (2004) Copper mediates dityrosine cross-linking of Alzheimer's amyloid-β, *Biochemistry 43*, 560−8.
42. Kadlcik, V., Sicard-Roselli, C., Tony, A. Mattioli, T. A., Kodicekz, M., and Houée-Levin, C. (2004) One-electron oxidation of β-amyloid peptide: Sequence modulation of reactivity, *Free Radical Biol. Med. 37*, 881−91.
43. Fancy, D. A., and Kodadek, T. (1999) Chemistry for the analysis of protein-protein interactions: rapid and efficient cross-linking triggered by long wavelength light, *Proc. Natl. Acad. Sci. U.S.A. 96*, 6020−4.
44. Bitan, G., and Teplow, D. B. (2004) Rapid photochemical cross-linking—a new tool for studies of metastable, amyloidogenic protein assemblies, *Acc. Chem. Res. 37*, 357−64.
45. Vollers, S. S., Teplow, D. B., and Bitan, G. (2005) Determination of peptide oligomerization state using rapid photochemical crosslinking, *Methods Mol. Biol. 299*, 11−8.
46. Fancy, D. A., and Kodadek, T. (1998) A critical role for tyrosine residues in His6Ni-mediated protein cross-linking, *Biochem. Biophys. Res. Commun. 247*, 420−6.
47. Lazo, N. D., Grant, M. A., Condron, M. C., Rigby, A. C., and Teplow, D. B. (2005) On the nucleation of amyloid β-protein monomer folding, *Protein Sci. 14*, 1581−96.
48. Bitan, G., Kirkitadze, M. D., Lomakin, A., Vollers, S. S., Benedek, G. B., and Teplow, D. B. (2003) Amyloid β-protein (Aβ) assembly: Aβ40 and Aβ42 oligomerize through distinct pathways, *Proc. Natl. Acad. Sci. U.S.A. 100*, 330−5.
49. Bitan, G., Lomakin, A., and Teplow, D. B. (2001) Amyloid β-protein oligomerization: prenucleation interactions revealed by photo-induced cross-linking of unmodified proteins, *J. Biol. Chem. 276*, 35176−94.
50. Gross, A. J., and Sizer, J. W. (1959) The oxidation of tyramine, tyrosine, and related compounds by peroxidase, *J. Biol. Chem. 234*, 1611−4.
51. Lehrer, S. S., and Fasman, G. D. (1967) Ultraviolet irradiation effects in poly-Ltyrosine and model compounds. Identification of bityrosine as a photoproduct, *Biochemistry 6*, 757−67.
52. Malencik, D. A., and Anderson, S. R. (2003) Dityrosine as a product of oxidative stress and fluorescent probe, *Amino Acids 25*, 233−47.
53. Schägger, H., and von Jagow, G. (1987) Tricine-sodium dodecyl sulfate-polyacrylamide gel electrophoresis for the separation of proteins in the range from 1 to 100 kDa, *Anal. Biochem. 166* (2), 368−79.

BI0605585